




Article

Concept Design of a High-Voltage Electrostatic Sanitizer to Prevent Spread of COVID-19 Coronavirus

Vahid Behjat ^{1,2,*} , Afshin Rezaei-Zare ², Issouf Fofana ¹  and Ali Naderian ³ 

- ¹ Modelling and Diagnostic of Electrical Power Network Equipment Laboratory (MODELE), Department of Applied Sciences, Université du Québec à Chicoutimi, Chicoutimi, QC G7H 2B1, Canada; ifofana@uqac.ca
- ² Department of Electrical Engineering and Computer Science, York University, Toronto, ON M3J 1P3, Canada; rezaei@yorku.ca
- ³ High-Voltage Department, METSCO Energy Solution, Toronto, ON L4K 5W1, Canada; Ali.naderian@metsco.ca
- * Correspondence: Vahid.Behjat1@uqac.ca

Abstract: In addition to public health measures, including social distancing, masking, cleaning, surface disinfection, etc., ventilation and air filtration can be a key component of a multi-pronged risk mitigation strategy against COVID-19 transmission indoors. Electrostatic precipitators (ESP) have already proved their high performance in fluid filtration, particularly in industrial applications, to control exhaust gas emissions and remove fine and superfine particles from the flowing gas, using high-voltage electrostatic fields and forces. In this contribution, a high-voltage electrostatic sanitizer (ESS), based on the electrostatic precipitation concept, is proposed as a supportive measure to reduce indoor air infection and prevent the spread of COVID-19 coronavirus. The finite element method (FEM) is used to model and simulate the proposed ESS, taking into account three main mechanisms involving in electrostatic sanitization, namely electrostatic field, airflow, and aerosol charging and tracing, which are mutually coupled to each other and occur simultaneously during the sanitization process. To consider the capability of the designed ESS in capturing superfine particles, functional parameters of the developed ESS, such as air velocity, electric potential, and space charge density, inside the ESS are investigated using the developed FEM model. Simulation results demonstrate the ability of the designed ESS in capturing aerosols containing coronavirus, precipitating suspended viral particles, and trapping them in oppositely charged electrode plates.



Citation: Behjat, V.; Rezaei-Zare, A.; Fofana, I.; Naderian, A. Concept Design of a High-Voltage Electrostatic Sanitizer to Prevent Spread of COVID-19 Coronavirus. *Energies* **2021**, *14*, 7808. <https://doi.org/10.3390/en14227808>

Academic Editor: William G. Dunford

Received: 27 October 2021

Accepted: 17 November 2021

Published: 22 November 2021

Publisher's Note: MDPI stays neutral with regard to jurisdictional claims in published maps and institutional affiliations.



Copyright: © 2021 by the authors. Licensee MDPI, Basel, Switzerland. This article is an open access article distributed under the terms and conditions of the Creative Commons Attribution (CC BY) license (<https://creativecommons.org/licenses/by/4.0/>).

Keywords: electrostatic sanitizer; coronavirus; COVID-19; finite element modeling

1. Introduction

Nowadays, indoor air quality (IAQ) issues are becoming a crucially important subject for human health, especially in the context of the recent COVID-19 disease pandemic [1,2]. Since COVID-19 is a respiratory disease, to prevent transmission of its causing agents, health organizations, including the World Health Organization (WHO) and US Centers for Disease Control and Prevention (CDC), have recommended specific airborne precautions. In this regard, several guidelines have been issued on keeping physical distance with people that have a fever, cough, and general symptoms of the disease, besides the importance of personal hygiene etiquette [3–6]. However, these measures seem to not be sufficient enough to prevent the spread of the deadly virus.

The transmission of the COVID-19 virus occurs mainly via droplets during close contact or touching infected surfaces [7–10]. It may also transmit through aerosols, as it has been pointed out in several research studies [11–16]. In this regard, some research has focused on how poor indoor air quality amplifies the effects of airborne viruses, including the COVID-19 coronavirus [17]. One of the most important strategies to address this

issue is using indoor air filtration and purification devices, besides the air ventilation systems [18–20].

To control the spread of COVID-19, it is important to have an idea about the transmission routes of the infectious agent. For almost every respiratory virus disease, three transmission routes are more dominant: (1) direct transmission of viruses in close contact region with the patient through droplets emitted while sneezing, coughing, singing, shouting, talking, and breathing; (2) indirect transmission via the surface contact through hand–hand, hand–surface, etc., contacts; and (3) long-range airborne transmission via aerosols [11,21]. While physical distancing is important to avoid close contact, in the case of the latter item, the overall risk of long-range aerosol concentration over several meters onward from an infected person is still there and can be reduced with adequate ventilation and effective air filtration solutions [11].

With regard to the size and how long respiratory droplets can remain suspended in the air, they are divided into two basic categories: large and small droplets. Large particulates, which are named as “droplets”, often refer to droplets $>5\ \mu\text{m}$ in diameter. They fall rapidly to the ground under gravity and are, therefore, transmitted only over a limited distance (e.g., $\leq 2\ \text{m}$). In contrast, droplets $\leq 5\ \mu\text{m}$ in diameter are referred to as “aerosols”, and they can remain floating in the air for significant periods of time and can transmit over long distances [5,22]. In fact, the dissemination of aerosols causes the spread of the infectious agents, defined as airborne transmission. It should be pointed out that the definition for “large” and “small” droplets size range may be slightly different in some studies [23–25]. The distribution of aerosols in indoor environments has also been simulated using numerical methods in some research studies [26–30].

Another aspect associated with indoor airborne transmission of COVID-19 is that most patients spend the majority of their time in enclosed areas, and the room air can be saturated with airborne particles exhaled during breathing. Even in airborne infection isolation (AII) rooms, which are specifically designed to prevent the spread of droplet nuclei expelled by a patient, despite negative pressure isolation conditions, air currents that occur due to the door opening can cause a breakdown in isolation conditions; as a result, the pathogen can escape from the room and spread infection outside the room [25,31]. Indoor transmission of COVID-19 can occur rapidly after one individual is infected. The pathogen may then be inhaled by others who are nearby or may be some distance away from the source patient in a different or the same room that the patient has left, if there has not been sufficient air filtration and sanitization [32]. With all these observations, the use of proper ventilation and sanitization in indoor settings is crucial to reduce airborne contaminants, including the virus causing COVID-19 [33]. Air sanitizers and purifiers are generally designed to clean pollutants or contaminants out of the air that passes through them. Air cleaning and filtration can help reduce airborne containing viral particles. The reduction of airborne particles, by collection in the air cleaning devices, can also dramatically reduce the deposition of viral particles on surfaces that are necessarily or inadvertently touched [34,35].

Technologies that are used for particle reduction of indoor air include mechanical filtration, electret filtration, and electrostatic precipitators [36]. The traditional mechanical filtration, such as high-efficiency particulate air filters (HEPA), are composed of fine fibers or some porous materials, which mainly capture dust particles by means of blocking, inertia, and diffusion. However, the fibrous filters need to be replaced frequently, and with the accumulation of more collected particles, the air pressure drop will be increased. This operation consumes more power and energy and will be costly. To improve the traditional mechanical filter efficiency to make it able to get fine particles, decrease the effect on air resistance, reduce the energy consumption of the filter, and prolong the service life, electret filters have been proposed to combine the electrostatic effect with the fibrous filter. The electrical charges on the fibers increase the electrostatic attraction forces [37,38]. However, it should be noted that, despite the high efficiency rates of the electret filter’s initial filtration, efficiency decreases over time due to the charge decay [39]. Electrostatic precipitators

(ESPs) use high voltage for air ionization and electric charging of the particles to trap them with electric forces [20].

Comparing ESP vs. HEPA, the efficiency of HEPA filters in capturing airborne particulates is almost the same for all the particles that are as small as $0.3\ \mu\text{m}$ in diameter. In contrast, the collection efficiency of electrostatic sanitizers is dependent on the size of the airborne loads and can reach up to 95–98% for the smallest particles ($0.3\text{--}2.5\ \mu\text{m}$) and 99% for the largest particles ($>2.5\ \mu\text{m}$) [40,41]. High efficiency in removing fine particles, along with the ability to purify large amounts of incoming gas, and low maintenance cost are the main advantages of ESPs over other filtering equipment [42–44]. That is why electrostatic precipitators are considered as one of the most promising ways to remove particles from exhausted gases in many industrial processes [45–48]. They are used in electric power plants, paper mills, cement, steel industry, and chemical industry and have two main uses (depending on the specific industry): reduction of air pollution in the environment and collection of dust particles for reuse [49,50].

The basic principles governing the operation of electrostatic precipitators are relatively straightforward; hence, they are well described in the literature [51–55]. It has been discussed the collection efficiency of precipitators as a function of some parameters, such as the type of supply voltage, design of the precipitator, arrangement of discharge wires and collecting plates, speed distributions of dust particles in the precipitator, dust resistivity and particles sizes, maintenance mode of precipitators, and changes that occur during operation [56–58]. It has been focused on the simulation of the electric potential and field strength in ESPs [59,60]. The simple interior structure of a one-stage wire–plate electrostatic precipitator with a single discharging electrode is shown in Figure 1. The unclean air, with viral and other contaminants, enters the ESP via the inlet and passes through a channel that contains grounded collecting plates and a discharging electrode. A high electrical potential is applied to the electrode, which induces a corona discharge, and ionizes the surrounding air. Corona discharge, which is the main mechanism of ESP to ionize the air, is still considered a challenging problem [61]. It has modeled this phenomenon by coupling electrostatic and electrokinetic problems [62,63]. After the particle charging and attraction process, some of them are deposited on the collecting plates and others are driven out through the outlet by the airflow. The air velocity in crossing the channel, the number and geometrical shape of the discharging electrode/s, distance of the collecting plates from the electrode/s, and the electric field intensity inside the channel are the key factors that affect sanitizer efficiency in removing the viral particulates.

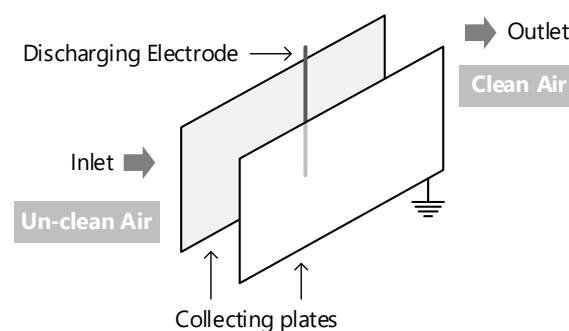


Figure 1. A 2D schematic of the electrostatic precipitator (ESP). The device consists of an air inlet, air outlet, and body housing the discharging electrode and collecting plates.

Human’s emitted respiratory particles can vary from 0.1 to more than several tens of micrometers in diameter, in the form of aerosols and droplets [63–65]. In indoor air and under common conditions, COVID-19 viruses can remain active even for an unlimited time and transmit with airflow [11,31,32]. ESPs with various designs have been widely applied in industrial applications; however, to adapt them for indoor air treatment, some concerns, such as high efficiencies for collecting fine particles, should be addressed [19].

This study intends to develop a high-voltage electrostatic sanitizer (ESS) with the ability to collect superfine viral contaminant particles. For the purpose of this study, first, the characteristics of droplets containing coronavirus are discussed to lay the groundwork for the modeling and simulation process. The structure of the proposed electrostatic sanitizer and its working principle is considered in the next section. Following this section, theoretical foundations to model the electrostatic field, particle charging, and airflow dynamics are extracted. A numerical model of the sanitizer is developed using 2D FEM modeling, by employing Maxwell and compressible Navier–Stokes equations. Then, the results of the numerical modeling, along with their discussion, are provided. Future directions of the research, to develop a detailed design of the sanitizer, and conclusions are given at the end.

2. Viral Load Properties

According to research findings, the main vehicle for airborne respiratory disease transmission is the droplet exhaled by the infected person [66]. Respiratory droplets are produced during normal breathing, speaking, coughing, or sneezing with a wide span of sizes and quantities [11,67]. The droplets expelled by a person consist mostly of water (almost 98%), with various inclusions (e.g., Na^+ , K^+ , Cl^-), and their size varies from aerosols with diameters $<1 \mu\text{m}$ to large droplets with diameters up to $600 \mu\text{m}$. It should be pointed out that the size and motion of the particle depends on the generation process, such as exhaled air velocity and the viscosity of the fluid, as well as environmental conditions, such as relative humidity, the ambient air temperature, and the direction and strength of local airflows [68–76]. Large droplets are significantly affected by gravity and deposit rapidly on the floor or other surfaces [77]. However, light particles (aerosols), containing the virus, can stay in the air for a long time and transport over longer distances; they could infect other people via the mouth, nose, and eyes if they do not use adequate personal protective equipment [26,27].

Due to evaporation, both the size and mass of the droplet change. According to research findings in [66], under normal air conditions, droplets smaller than $100 \mu\text{m}$ in diameter would completely dry out before falling to the ground, in approximately 2 m distance. This means that droplets could transform into aerosols by evaporation before settling [78–80]. The overall size of aerosols also depends on the saliva's organic and inorganic contents, and the ultimate limit in size is the diameter of the virus itself, which is about $0.14 \mu\text{m}$ [81]. Figure 2 shows how a respiratory droplet within the liquid phase evaporates under environmental conditions and eventually creates an aerosol filled with viruses and other contaminants [82].

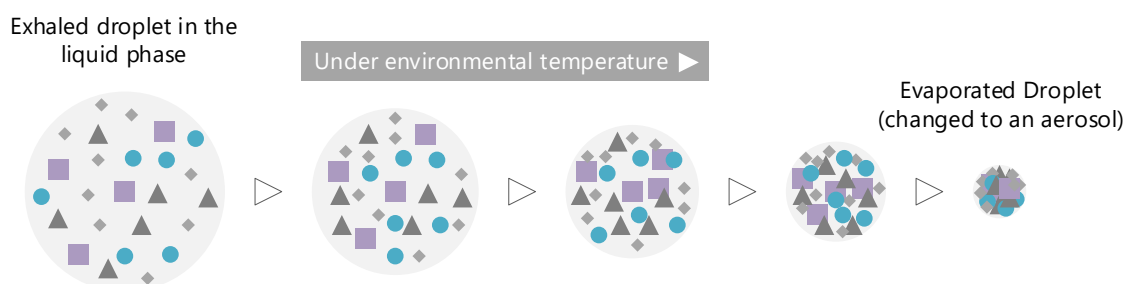


Figure 2. Evaporation of a human exhaled droplet in the liquid phase to a non-evaporative aerosol containing viruses.

Any movement of the air may carry indoor floating aerosols. Airstreams are created simply from the air temperature differences, even from human body heat. In the same way, other mechanical and electrical devices, including fans, televisions, and medical equipment, can disturb patients' nearby airflows and move the viruses in a closed room. Another point, in this regard, is the droplet's speed, which can reach up to 15 km/h while coughing [83]. However, the parameters that affect the ESS efficiency are the particle size (and its electric

properties) and the particle velocity inside the ESS channel, which completely depends on the device's mechanical fan speed and other operational and structural parameters.

3. Principles of Operation

The precipitation of particles under an electric field involves complex mechanisms in the collection process and different parameters, including particle size, particle chemical composition, charge-to-mass ratio, airflow velocity inside ESS, electrical parameters, and operating conditions, which affect particle attraction to the collection plates. Therefore, this section will focus on the basic operational principles of ESP to develop a high-voltage electrostatic sanitizer design scheme that is able to remove viral particles from the air, especially particles containing COVID-19 viruses. In summary, aerosols and the particle collection process (from the air using ESS) can be expressed in the following three steps: particle charging by produced ions and electrons, particles move towards the collecting plates under electric force, and particle deposition on collecting plates [35].

To produce a high electric field in the ESS, a discharging wire electrode is typically placed between two collecting plates. Collecting plates are electrically grounded (have zero potential), and high voltage is applied to the wire. The electric field in an ESS can be generated with either negative or positive high voltage. However, under the same conditions, the negative voltage is generally used because the ESS can be operated at a higher voltage before spark-over, compared to the positive electric field. The electric field has its maximum value close to the discharge electrode and rapidly decreases moving toward the collecting plate [84,85].

Based on Katpsov's hypothesis about smooth wire electrode structure, as the electrode voltage increases, the electric field increases proportionally until the applied voltage reaches to the onset voltage. The onset voltage is the value of the voltage applied to the stressed wire electrode, where corona discharge takes place and free electrons are being produced. After that, the electric field will preserve its value [86]. Figure 3 demonstrates the electric field strength versus applied electric voltage at the discharging electrode for the charge-free case without ionization and for the corona case. The strength of the electric field is mainly dependent on the wire electrode and collecting plates' geometrical properties. Other environmental parameters, such as temperature, pressure, and humidity can also affect electric field value, as they can affect ion mobility in the air [18].

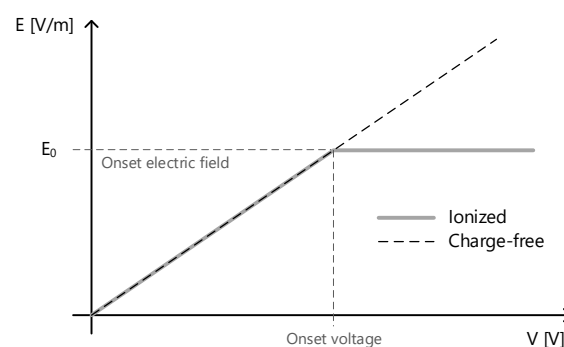


Figure 3. Overview of the electric field strength versus applied electric voltage at the discharging electrode.

The onset electric field at the wire electrode can be obtained using Peek's law [87]:

$$E_0 = 3.1 \times 10^6 \delta (C_1 + C_2 / \sqrt{\delta r_i}) \quad (1)$$

where E_0 (SI unit: V/m) is the onset electric field, δ is the relative air density normalized to real temperature and pressure conditions, r_i is the radius of the wire electrode (SI unit: m), $C_1 = 1$ (SI unit: V/m), and $C_2 = 0.031$ (SI unit: V/m).

At the start point of the ESS operation, it needs to generate electric charges in the sanitizer. Under a strong electric field, electrons can be separated from the air atoms and

create positive ions and free electrons. A neutral atom of air crossing the active region (the region around the discharging electrode where the electric field is strong) is ionized and a positive ion and free electron are created. These created free electrons and positive ions are accelerated by the negative electric field in opposite directions, are separated from each other, and get kinetic energy. The electron has a much higher charge-to-mass ratio; so, it is accelerated to a higher velocity than the positive ion. It gains enough energy from the field, and when it crashes to another atom, knocking out another electron, it ionizes it and creates another positive ion. These electrons are accelerated and collide with other atoms, creating a further electron and positive ion pairs, and then collide with more atoms [88,89]. This process, named as avalanche multiplication, is repeated many times, so that large quantities of free electrons and positive ions are formed within the sanitizer channel. Figure 4 depicts the air ionization process under the strong electric field.

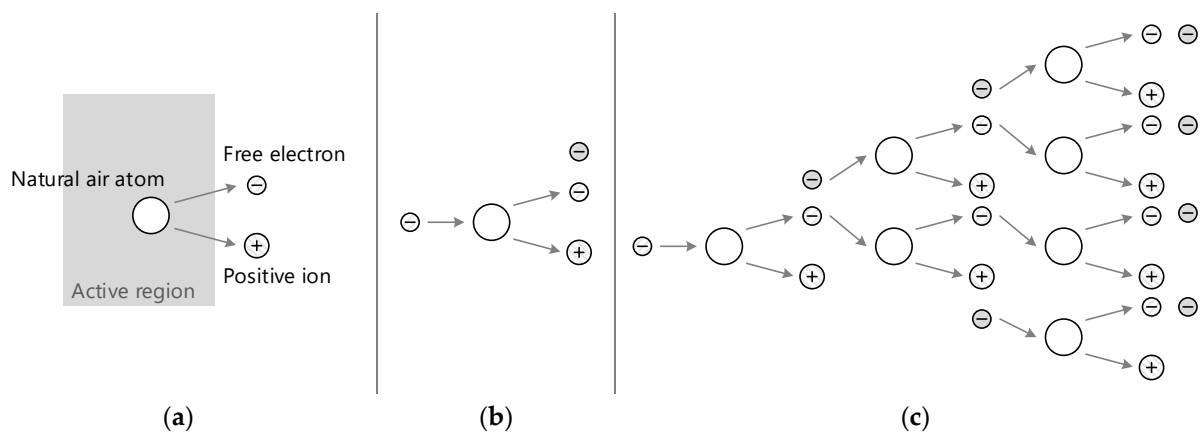


Figure 4. Electrical charge production. (a) Ionization of an air atom. (b) Colliding accelerated free electrons to another air atom and bumping another electron from the atom. (c) Ascending production of electrons and positive ions.

On the other hand, the big positive ions that move slowly toward the negative discharge electrode (under attractive forces) pick up speed, and many of them collide right into the discharging electrode or the air around the wire, which causes additional electrons to be knocked off. This process is called secondary emission [88,89].

As the electrons move away from the strong electrical field area, their velocity starts to slow down; they are still repulsed by the negative electric field but to a lesser extent. They collide with other air atoms, but instead of violently colliding with them, the electrons reach the air atoms and are captured by them, as shown in Figure 5. This action gives up a negative charge to the air atoms and creates negative air ions. Because the ions are negative, they move in the direction opposite the strong negative field, toward the collecting plates. Along with free electrons, these negative air ions play a key role in capturing the particles [42].

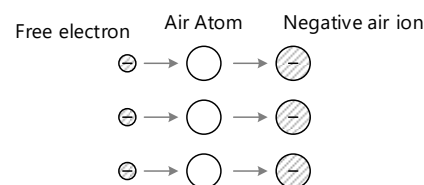


Figure 5. Formation of negative air ions.

The created free electrons and negative ions should cross along the path of the electric field, in order to reach the closest grounded plate. Thus, a current of electrons is formed from the discharge wire towards the collecting plates [43]. Aerosols and particles are charged by these generated electrons and ions as they pass through the sanitizer channel

and dragged toward the collecting plates by the electric field action (Coulomb Forces). When the charged particles arrive at collecting plates, they lose their electric charge through the ground connection while they remain on the plates [90]. A simple demonstration of ESS operation is sketched in Figure 6.

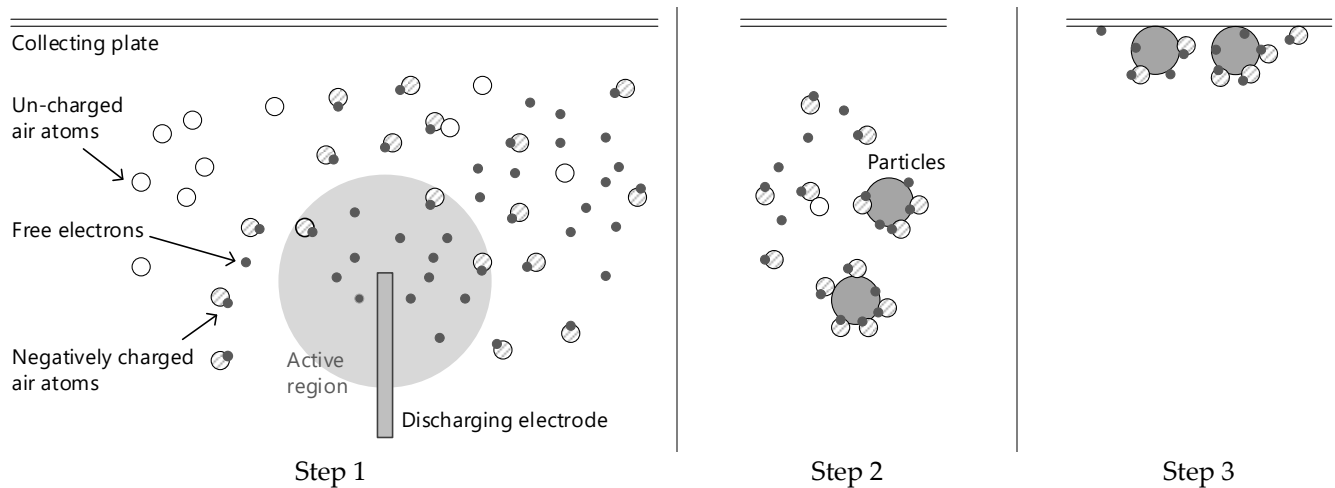


Figure 6. The ESS operation in collecting the particles from the air.

The particles at the entrance of the sanitizer are uncharged. However, when they are moving toward the grounded collecting plates, they are negatively charged and their charge increases; so, the large number of free electrons and air ions can fit on them. It is worth mentioning that droplets can absorb more charges than aerosols because of their large dimensions. Eventually, at a point called the saturation charge level, the particles are so charged that they emit their own negative electrical field, and this negative electric field around the particles repulses the electrons and negative air ions and prevents the additional charges that are acquired [89].

Particle charging inside the electrostatic sanitizer is done by two mechanisms: field charging and diffusion charging, depending on the particle size. Field charging occurs when large particles (droplets) enter the electric field and cause a local displacement of the electric field lines. They change the local electric field distribution lines and drive the charges to continue to collide with them until they reach the saturation charge level. After that, they divert electric field lines away from themselves and prevent absorbing new charges, as shown in Figure 7.

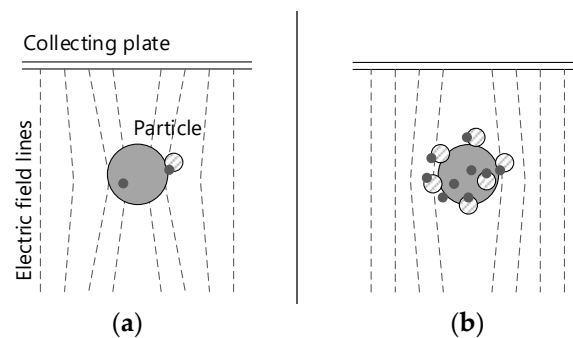


Figure 7. Particle charging by the field mechanism, and its effect on the electric field lines; (a) unsaturated particle; (b) saturated particle.

Diffusion charging is based on random Brownian motion, and the collision of particles with electrons or air ions is directed by thermal effect. With increasing the temperature, the mobility of the air increases and more movement occurs [18]. The electrons and ions collide

with the particles because of their random thermal motion and give a charge to them. In the case of fine particles, they do not change the electric field line paths. Thus, diffusion charging is the only mechanism by which fine particles become charged [89]. Based on studies, if particle diameter is larger than 1 μm , then the field charging dominates, and if the particle diameter is less than 0.1 μm , diffusion charging dominates. Otherwise, two kinds of mechanisms exist [42].

Because of the aerosol small diameters, they are charged less than droplets or large particles and so, the amount of electric charge on them is very low [34,91]. Droplets (which have large diameters) are collected more efficiently, given that their displacement is mainly influenced by the electric field. On the contrary, besides the large droplets, very fine aerosols are also collected more efficiently because they are subjected to less airflow drag forces. Between these two extremes, larger aerosols behavior in ESS is quite different, as they usually move in straight lines with the air stream and with insufficient charging that consequently results in low collection efficiency for them [92].

The collection efficiency is normally defined as collected aerosol mass proportion to the overall mass entering the ESS over some time. Deutsch equation can be used for theoretical analysis of ESS efficiency under ideal conditions [52]:

$$\eta = 1 - \exp\left(-\omega \cdot \frac{A}{Q}\right) \quad (2)$$

where η is the collecting efficiency, ω is the charged particle migration velocity (SI unit: cm/s), A is the effective collecting plate area (SI unit: m^2), and Q is the gas flow rate through the sanitizer channel (SI unit: m^3/s). The particle migration velocity is the speed at which a particle, once charged, moves toward the grounded collection plates and depends on the particle size and shape, electric field strength, gas composition, temperature, etc. The A/Q term in the Deutsch equation is defined as specific collection area (SCA), which indicates the ratio of collection plates area over the air volume flow of the sanitizer [93]. The value of SCA has a direct relation with particle residence time inside the sanitizer. The residence time for a particle is the time interval when the particle is entered into the ESS and subjected to the electrostatic field, and all the ESS processes, including charging, migration, and collection, occur in this period. The longer the residence time, the more charge will accumulate on the particles [94].

To increase sanitizer efficiency, in order to make it able to collect fine and large aerosols together, both the collection area and the applied high voltage must be designed for best performance. A possible solution to make it easier to capture aerosols is increasing their charging, which can be done by increasing the applied voltage on the discharging electrode. However, increasing the electric field can affect the airflow paths and create electrohydrodynamic ion wind in the sanitizer. This event can cause severe turbulence that makes the aerosol collection even more difficult and may pull them back into the airflow before they arrive at the collecting plates [92]. Hence, optimized electric field strength must be adjusted in a way that the ion wind is not so strong, and the fine particle collection efficiency can reach its maximum value. Another issue in adjusting the applied voltage is that increasing the applied voltage will increase the field strength and ion formation until spark-over happens. Spark-over refers to internal sparking between the discharging electrode and collecting plates [95]. As a solution to this challenge, two-stage electrostatic precipitators, that separate the charging and collection stages, have been proposed [96–100]. In this structure, the voltage on the discharging electrode can be increased to higher values than one-stage ESS. Figure 8 shows the schematic view of a two-stage electrostatic sanitizer.

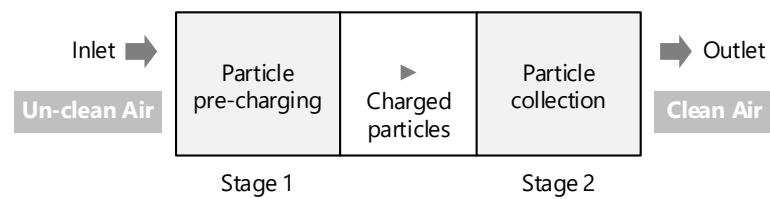


Figure 8. Schematic of a two-stage ESS.

One of the other methods to improve the aerosols collection efficiency is increasing the diameter of the particles via the agglomeration of them together or with large particles, such as water droplets. Agglomeration can be done by chemical methods, electrical methods, etc. [101–103]. Figure 9 shows the simple schematic of an electrostatic sanitizer with an electrical agglomeration system, consisting of a bipolar pre-charging unit, mixer, and ESS. Particles are positively or negatively charged in the pre-charging unit, agglomerated together in the mixer unit, and, finally, collected by the ESS. The mixer unit can have AC or DC high voltage. The modes of aerosol electrical agglomeration are shown in Figure 10.

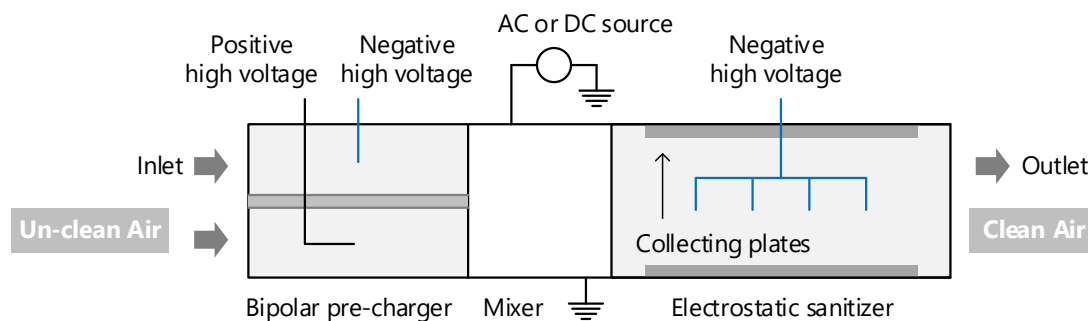


Figure 9. A simple schematic of ESS with agglomeration system.

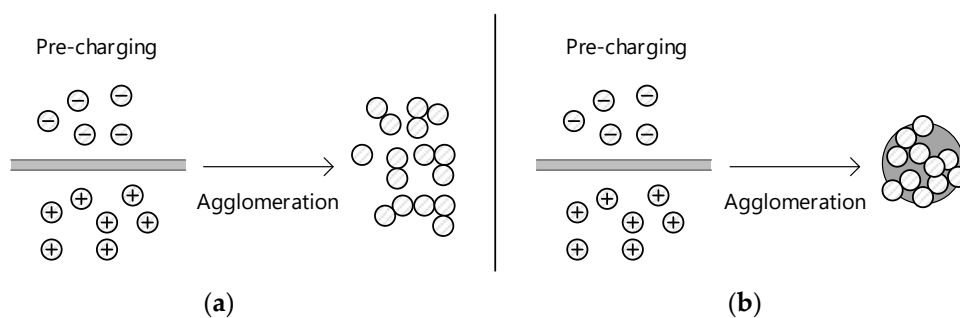


Figure 10. Aerosols electrical agglomeration; (a) agglomeration of small particles together; (b) agglomeration of small particles with the large particle.

Besides the ESS configuration, one of the most important factors affecting the collection efficiency is the aerosol resistivity. Resistivity is a function of particles' chemical composition. From the electrical point of view, resistivity is a particle's tendency to transferring charges. Particles can have high, normal, or low resistivity [89]. Environmental conditions, such as temperature and humidity, have a significant effect on particle resistance. Particles that have high resistance values are hardly charged; however, once charged, they do not easily get rid of their acquired charge when arriving at the collecting plates. On the opposite, particles with low resistivity easily get charged and readily release their charge to the grounded collecting plates. These particles may be easily apart from the plates and escape through the sanitizer with the airflow. In this regard, the air velocity into the sanitizer must be reduced enough to prevent re-entrainment of the particles [104].

4. Theoretical Foundations

For numerical modeling of the electrostatic sanitizer, three main mechanisms should be considered including electrostatic field, airflow, and aerosol charging and tracing. These physical phenomena are mutually coupled to each other and occur during the sanitizer operation (at the same time).

4.1. Electrostatic Field

Applying high voltage to the discharging electrodes and connecting the collecting plates to the ground potential produces corona discharge, which in turn generates space charges and a continuous electric current flowing between electrodes and plates. The electrostatic field established this way, can be described by the well-known Maxwell's equations, Poisson, and charge conservation equations. Assuming steady-state conditions and ignoring the magnetic field influence, the electric field intensity inside the sanitizer can be described by Gauss's law [105–108]:

$$\nabla \cdot \vec{E} = \frac{\rho_q}{\varepsilon_0} \quad (3)$$

Relating the electric field to the potential with the equation $\vec{E} = -\nabla V$, gives the well-known Poisson equation as [108]:

$$\varepsilon_0 \nabla^2 V = -\rho_q \quad (4)$$

where E is the electric field intensity (SI unit: V/m), ρ_q (SI unit: C/m³) is the space charge density, ε_0 is the vacuum permittivity, and V is the electric potential (SI unit: V). Moving ionic charges towards the grounded plates, create an electric current with a density defined as:

$$\vec{J} = \mu \rho_q \vec{E} + \rho_q u - D \nabla \rho_q \quad (5)$$

The three terms on the right side of Equation (5) are drift current, due to electric field, convection current under the airflow, and diffusion current, respectively. Under stationary conditions, the quantity of electric charge in the sanitizer channel do not change; thus, the current density must satisfy the charge conservation equation:

$$\nabla \cdot \vec{J} = 0 \quad (6)$$

where J (SI unit: A/m²) is the current density, μ (SI unit: m²/V·s) is the ion mobility, u is the fluid (air) velocity (SI unit: m/s), and D is the ion diffusion coefficient (SI unit: m²/s). This set of equations after manipulation, give the following transport equation:

$$\mu \left(\frac{\rho_q^2}{\varepsilon_0} - \nabla V \cdot \nabla \rho_q \right) + \nabla \rho_q \cdot u - D \nabla^2 \rho_q = 0 \quad (7)$$

4.2. Airflow (Laminar Flow)

At the inlet of the sanitizer, the aerosols are primarily under the impression of the air convection forces. So, studying the laminar flow field characterization is the initial step for the prediction of aerosol behavior in the sanitizer. Due to the small air pressure drop, along with the sanitizer, the air is considered as an incompressible Newtonian fluid; so, the density and viscosity are considered constant. The Navier–Stokes equations, which are a statement of Newton's second law of motion, are used to solve for the air velocity and pressure. The airflow can be described by the two basic governing equations for the conservation of the mass and momentum, the following Equations (8) and (9), respectively:

$$\nabla \cdot \vec{u} = 0 \quad (8)$$

$$\rho(\vec{u} \cdot \nabla)\vec{u} = \nabla \cdot [-PI + \mu(\nabla\vec{u} + (\nabla\vec{u})^T)] + S \quad (9)$$

where μ is the air viscosity (SI unit: kg/(m·s)), ρ is the air density (SI unit: kg/m³), P is the air pressure (SI unit: Pa), and S is the source term due to the electric field and defined as [109]:

$$S = \rho_q \vec{E} \quad (10)$$

4.3. Aerosol Tracing

In the sanitizer channel, aerosols are affected by combined forces of gravity, electric force, and airflow aerodynamic drag forces. The aerosol (particle) positions can be computed by solving second-order equations of motion for the aerosol position vector components, using Newton's second law [109]:

$$\begin{aligned} \frac{dx_p}{dt} &= v \\ \frac{d}{dt}(m_p \vec{v}) &= \vec{F}_t \end{aligned} \quad (11)$$

where x_p is the aerosol position (SI unit: m), v is the aerosol velocity (SI unit: m/s), m_p is the aerosol mass (SI unit: kg), and F_t is the total force (SI unit: N) that acts on the aerosols. In this study, two air drag forces and the electric force are considered and the gravitational forces are neglected. The electric force exerted on the aerosols is defined as [108,109]:

$$\vec{F}_e = \frac{\vec{E} q_p}{m_p} \quad (12)$$

where \vec{E} is the electric field intensities and q_p is the electric charge of the aerosol that is the sum of aerosol charges due to both diffusion and field mechanisms. The aerosols entering the ESS are assumed to be spherical in shape and neutral in charge. The charge accumulated on the aerosols is computed by the following equation:

$$\tau_c \frac{dq_p}{dt} = \begin{cases} R_f + f_a & |v_e| \leq |v_s| \\ R_d f_a & |v_e| > |v_s| \end{cases} \quad (13)$$

where τ_c is the charging time constant, v_e is the aerosol electric charge, and v_s is the aerosol saturation charge. With regard to Equation (13), it can be seen that aerosol charge is increasing over time while it is crossing the sanitizer channel. Diffusion charging never reaches a limit, but it becomes very slow with time. The charging time constant (τ_c) is described as:

$$\tau_c = \frac{e^2}{4\pi\rho_q\mu k_B T_i} \quad (14)$$

where k_B is the Boltzmann constant, T_i is the ion temperature, R_f and R_d are the dimensionless charging rates due to field and diffusion transport, respectively, defined as:

$$R_f = \frac{v_s}{4\pi\epsilon_0} \left(1 - \frac{v_e}{v_s}\right)^2, \quad R_d = \frac{v_e - v_s}{\exp(v_e - v_s) - 1} \quad (15)$$

and

$$v_e = \frac{Ze^2}{4\pi\epsilon_0 r_p k_B T_i}, \quad v_s = 3\omega_e \frac{\epsilon_r}{\epsilon_r + 2} \quad (16)$$

$$\omega_e = \frac{er_p|E|}{k_B T_i} \quad (17)$$

where ε_r is the relative permittivity of each aerosol, Z is the accumulated charge number on aerosols, and e is the electronic charge (1.6×10^{-19} C) which $q_p = Ze$. To join the diffusion and field charging rates, the parameter f_a is used and defined as [109]:

$$f_a = \begin{cases} \frac{1}{(\omega_e + 0.475)^{0.575}} & \omega_e \geq 0.525 \\ 1 & \omega_e < 0.525 \end{cases} \quad (18)$$

where \vec{F}_D the drag force from airflow and for aerosols is defined, as follows:

$$\vec{F}_D = \frac{1}{\tau_p s} m_p (\vec{u} - \vec{v}) \quad (19)$$

where τ_p is the aerosol velocity response time (SI unit: s) and is defined as:

$$\tau_p = \frac{4\rho_p d_p^2}{3\mu C_D \text{Re}_r} \quad (20)$$

where ρ_p is the density of the aerosols (SI unit: kg/m³), d_p is the aerosol diameter (SI unit: m), C_D is the drag coefficient which depends on the aerosols Reynolds number, s is the drag correction coefficient, and Re_r is the relative Reynolds number given by the following equation:

$$\text{Re}_r = \frac{\rho_p d_p |u - v|}{\mu} \quad (21)$$

The above acquired equations clearly indicate that the forces acting on the aerosols are dependent on their physical and electrical properties (like mass, shape, size, resistivity, permittivity), electric field intensity inside the sanitizer, aerosol velocity, operating conditions (like temperature), and so on. The whole sanitizer mechanisms, such as the aerosol charging process and aerosol motion, are mutually coupled. Considering all parameters is crucial to properly model and obtain the optimized design and achieve the highest collection efficiency.

An algorithm was developed to take into account the coupling between different governing equations mentioned in this section. By applying a voltage higher than the onset value to the discharging electrodes, the electric field should be constant and equal to E_0 which is obtained using Peek's law. If this is not the case and the electric field is larger than E_0 , the space charge on the discharging electrodes is increased. Conversely, if the electric field is too small, the space charge is decreased. The solving process of Poisson and charge conservation equations is continued until the difference between E and E_0 is smaller than a predefined assumed tolerance and as a result, the distribution of space charge density and electric field intensity are obtained. After electrostatic simulation, the Coulomb force (term S in the airflow governing equation) is calculated as a product of the electric field and space charge density. The value of S is needed to simulate the airflow using the conservation of the mass and momentum equations. Because Equations (8) and (9) are nonlinear and coupled with each other, several iterations of the solution loop are performed before a converged solution is obtained. The airflow velocity is then entered back into the electrostatic simulation, which makes the whole simulation algorithm a triple iterative loop. The whole process is repeated until convergence is reached for all essential electrical and airflow parameters. Afterwards, detailed information of the electric field, electric potential, space charge distribution, and the airflow profile inside the sanitizer are obtained. In order to investigate the aerosol motion and tracing them, a number of aerosols with known physical and electrical specifications are released on the inlet. The aerosol motion is coupled with their charging process because the variation of the aerosol's charge, changes their path, which in turn affects their charging rate again because the electric field is not uniform inside the sanitizer channel. Aerosol tracing is done with the calculation

of aerosols charges and their position sequentially. At the end, a particle counter which is added at the outlet of the sanitizer is used to compute the aerosol collection efficiency.

5. Numerical Setup

To evaluate the capability of the ESS in capturing viral loads, a single-channel wire–plate type ESS with three wire electrodes is modeled and simulated. Figures 11 and 12 demonstrate the computational model domain with all dimensions and boundary conditions, respectively. The model consists of two flat collecting plates and three discharging wire electrodes are placed between them. The collecting plates are of 0.8 m in length with 0.1 m vertical space between them. The discharging wire electrodes which are 1 mm in diameter are placed in the channel between the collecting plates.

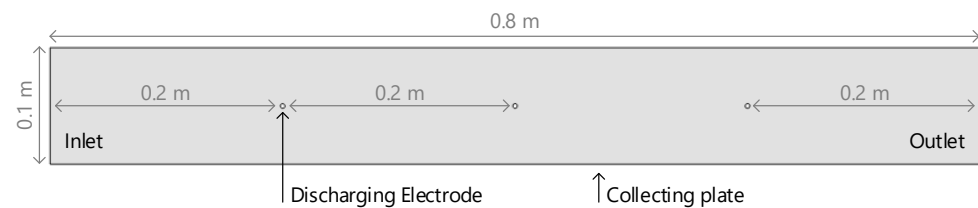


Figure 11. The computational domain of the modeled ESS (the electrodes are not to scale).

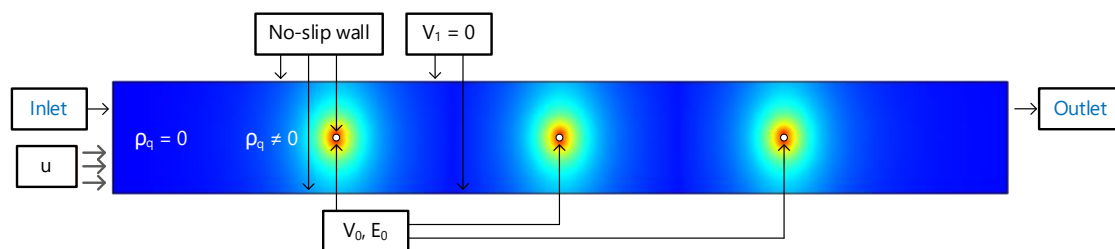


Figure 12. The computational domain boundary conditions.

With regard to the boundary conditions in order to properly determine the transport parameters, the boundary conditions for the wire electrodes and collecting plates potential are straightforward and can be defined directly: a given dc high voltage V_0 at the electrodes and $V_1 = 0$ at the plates (Dirichlet boundary conditions). However, boundary conditions for the electric potential V and space charge density ρ_q distribution in the sanitizer channel are indirect and should be calculated using Equations (4) and (7). Electric potential is obtained based on a known distribution of ρ_q using the Poisson equation and space charge density is obtained based on a known distribution of V using the current continuity equation. The value of space charge density on the surface of the electrodes is iterated until the electrode's electric field reaches the electric field onset value. In other words, the value of ρ_q is zero if $E_{(electrodes)} < E_0$ and $\rho_q \neq 0$ if $E_{(electrodes)} \geq E_0$.

The boundary conditions for the airflow are also straightforward: the two collecting plates and wire electrodes are defined as no-slip walls, and the air average velocity is defined as the inlet boundary. However, the boundary condition for the outlet is indirect and can be calculated using the Mass conservation equation. Boundary conditions used to solve this model have been summarized in Table 1.

Table 1. Boundary conditions applied to the ESS model.

	Electric Potential	Charge Density	Airflow	Particle Motion
Wire electrodes	$V = 30 \text{ kV}$	Peek's law	No slip	Reflect
Collecting plates	$V = 0 \text{ kV}$	$\nabla \rho_q = 0$	No slip	Trap
Inlet	$\nabla V = 0$	$\nabla \rho_q = 0$	$u = 1 \text{ m/s}$	$U = 1 \text{ m/s}$ Enter
Outlet	$\nabla V = 0$	$\nabla \rho_q = 0$	Mass conservation	Escape

The simulation of the model is carried out by employing COMSOL Multiphysics software and is conducted in three steps, as follows:

- (1) Stationary electrostatics simulation using an electrostatics module and PDE (partial differential equation) interface;
- (2) Stationary airflow simulation using laminar flow module;
- (3) Time-dependent aerosols motion using particle tracing for fluid flow module.

To compute the aerosols charging and relevant forces acting on them, the stationary study is used, which couples the electrostatic field, laminar flow, and particle charging processes together. Additionally, to compute the aerosols trajectory and obtain the collection efficiency of the ESS, the time-dependent study is used. The connection between the ESS electrostatics and fluid dynamics is established through the forces exerted on charged aerosols.

The aerosols that are injected into the computational domain at the inlet of the ESS are spherical in shape, with a diameter of 0.1–5 μm . The temperature and pressure of the air are set at 27 $^{\circ}\text{C}$ and 1 Pa, respectively, during the simulation. For the purpose of this study, saliva is considered as the aerosol with a density of 998 kg/m^3 . Aerosols are released on the left boundary and are collected at the walls.

6. Results and Discussion

To investigate the function of the designed ESS in capturing superfine viral loads, the distribution of air velocity, electric potential, and space charge density inside the ESS are considered using the developed FEM model. High voltage of -30 kV DC is applied to the electrodes and the air velocity at the inlet is 1 m/s. The computed airflow is illustrated by Figure 13, which shows the velocity profile of the model. As expected, the magnitude of the airflow velocity is zero near the collecting plates, while the velocity reaches its peak values near the discharging electrodes, as they are considered fixed and unaffected by the airflow.

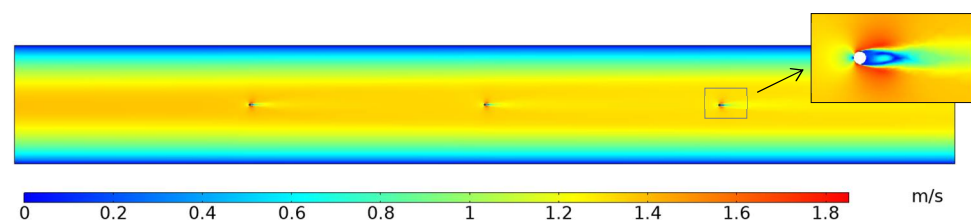


Figure 13. Velocity magnitude of the airflow inside the electrostatic sanitizer (ESS).

The distribution of electric potential and space charge density are depicted in Figures 14 and 15, respectively, where the electric field forms an elliptical region around the discharging electrodes. It can be observed from the figures that the space charge density is more intense near the electrodes and decreases as it moves toward the grounded collecting plates. Additionally, the electric field intensity around the electrodes is very strong and goes to zero near the plates. In this region (near the discharging electrodes), aerosols charge accumulation is done at a faster rate, due to the combined effect of large space charge densities and intense electric fields. The aerosols obtain electric charge as they move through the ESS channel, and most of them are trapped at the lowest distance to the discharging electrodes on the collecting plates.

From the sanitizer design point of view, and considering the simulation results with increasing the number of discharging electrodes, the average value of the drift force from the electric field and the space charge density are increased. So, it is expected that the efficiency of the ESS with more discharging electrodes reaches higher values, compared to a structure with lower discharging electrodes. Additionally, any increase in the applied voltage leads to increased electric corona, increased space charge density, increased electric field intensity, greater aerosols charging, and, finally, increased collection efficiency. In contrast, by increasing the airflow velocity, the aerosol residence time is decreased and, as

a result, the aerosols are less exposed to the electric field and can absorb less electric charge. On the other hand, increasing the air velocity means that the drag forces on the aerosols increase, which leads to the collection of fewer aerosols on the plates, and ultimately more aerosols escape the ESS, which causes decrease of particle removal efficiency.

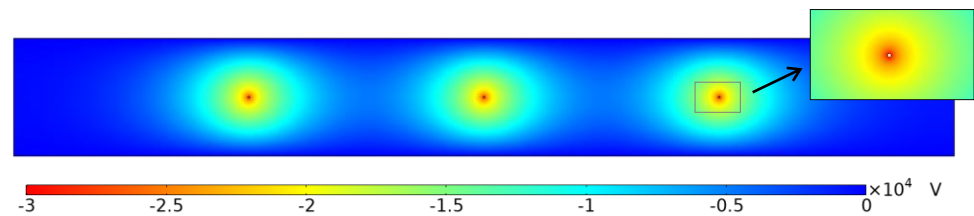


Figure 14. Electric potential contours in the ESS.

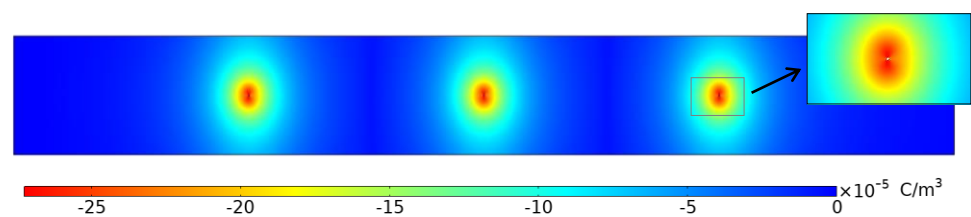


Figure 15. Space charge density contours in the ESS.

The results for aerosol tracing are represented in Figure 16 for a range of aerosol diameters between 0.1–5 μm . As expected, the fine aerosols are more collected, as they barely experience any air drag force. On the other hand, the biggest aerosols are more collected, due to their capability for holding higher charge, which leads to a greater Coulomb force; however, for the aerosols with intermediate diameter, the number of trapped aerosols is decreased.

Simulation results revealed the ability of the designed ESS in capturing superfine viral loads, such as COVID-19 particulates. Three main mechanisms, including electrostatic field, airflow, and aerosol charging and tracing, are coupled together to develop a concept design of an ESP being able to capture superfine particulates. Based on the acquired results, one can conclude that ESP can be utilized as a supportive measure to trap viral particulates, reduce indoor air infection, and prevent the spread of COVID-19 coronavirus. This contribution utilized a two-dimensional FEM model, in order to model and simulate ESS and study the feasibility of an electrostatic precipitation-based sanitizer in capturing viral loads. Three-dimensional FEM modelling could be a very time-demanding and challenging method in ESS design. However, it may guarantee more accurate results and provide more practical insights to a detailed design of an ESS, which would be in future scope of this work. Future work should also focus on considering and calculating the removal efficiency of the designed ESS with different structural and operational parameters and realization of a detailed design. Air flow patterns inside the sanitizer may be influenced by electrohydrodynamic flows, which was not considered in this work. For a detailed design of the ESS and its practical realization, future research may take this effect into account and consider its effect on the flow pattern and collection efficiency, particularly in the case of superfine particles.

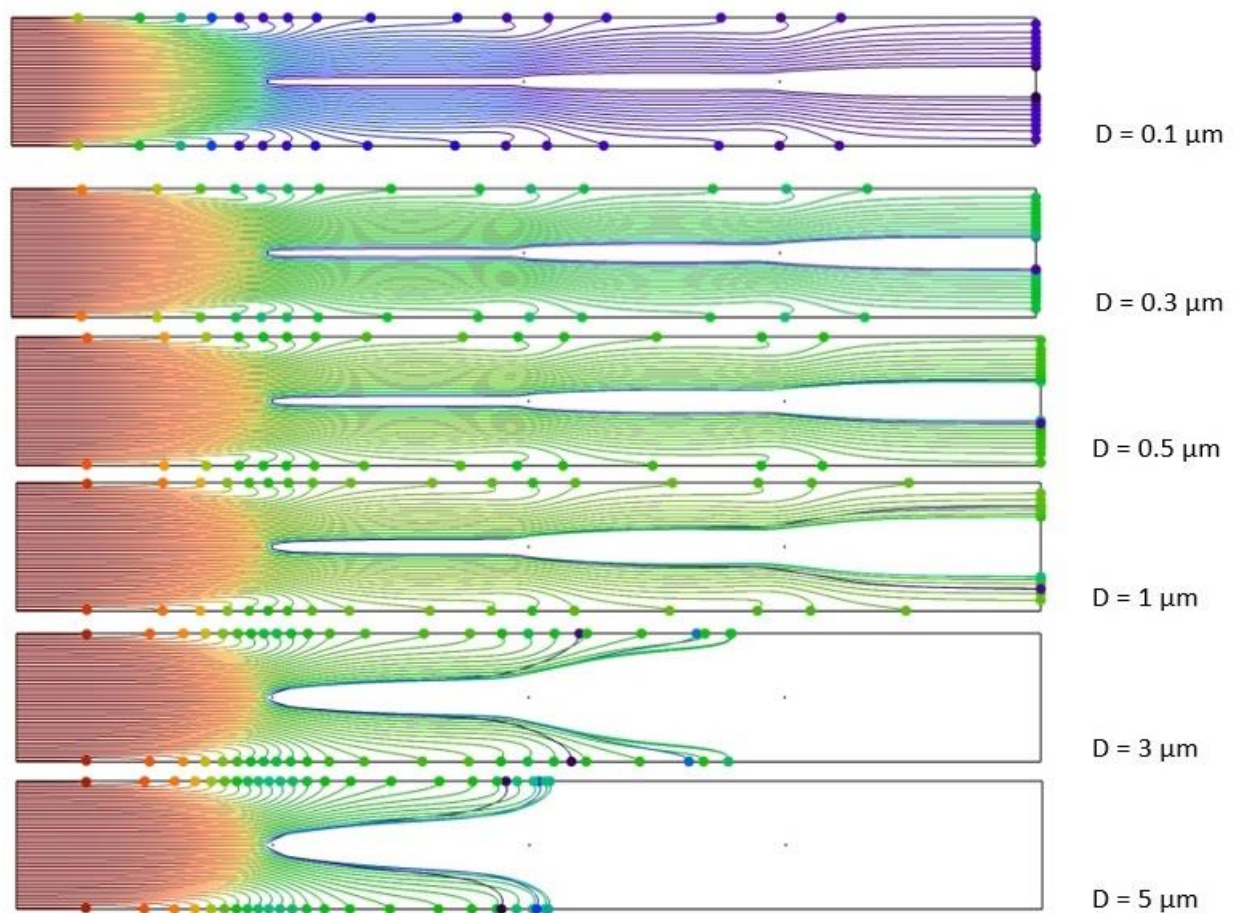


Figure 16. Aerosol trajectories through the ESS channel for aerosols with uniform diameters of, respectively, 0.1 μm , 0.3 μm , 0.5 μm , 1 μm , 3 μm , and 5 μm at $V = -30$ kV.

7. Conclusions

The main objective of this research work was to adapt the traditional ESP to reduce the indoor air pollution and, especially, prevent the spread of COVID-19 particulates. An electrostatic sanitizer was designed, modeled, and studied using the finite element method. The following subjects were discussed in detail: (a) study of human expelled droplets, in order to identify droplet transmission mechanisms and characterize them; (b) utilizing electric field to precipitate the suspended superfine particles from the air; (c) developing an algorithm to couple the governing equations of different mechanisms involved in electrostatic precipitation, including electrostatic field, airflow, and aerosol charging and tracing; and (d) proposing a simple electrostatic sanitizer by taking into account electrical and mechanical limitations. The research findings revealed the excellent performance of electrostatic precipitators to be used as air sanitizers for cleaning indoor air from the viral loads. Profile of air velocity, electric potential, and space charge density inside the designed ESS, obtained from FEM simulations, demonstrated the ability of the ESS in capturing superfine particles viral loads, such as COVID-19 particulates. It should be pointed out that by itself, air cleaning or filtration is not enough to protect people from exposure to viruses. However, when used supplementary, along with other practices (such as wearing masks, social distancing, frequent hand-washing, and surface disinfection), it can be part of a plan to reduce the potential for airborne transmission of COVID-19 indoors. Based on the findings in this study, the future work ought to focus on developing a detailed design of an electrostatic sanitizer to remove viral COVID-19 particulates. A detailed design may consider more aspects, such as the influence of electrohydrodynamic flows

inside the sanitizer and effect of the sanitizer's structural and operational parameters on the collection efficiency.

Author Contributions: Conceptualization, V.B., A.R.-Z., I.F. and A.N.; Formal analysis, V.B.; Investigation, V.B.; Methodology, V.B., A.R.-Z., I.F. and A.N.; Software, V.B.; Supervision, A.R.-Z. and I.F.; Validation, V.B.; Writing—original draft, V.B.; Writing—review & editing, V.B., A.R.-Z., I.F. and A.N. All authors have read and agreed to the published version of the manuscript.

Funding: This research work was supported by Alliance Grant (ALLRP) funded by the Natural Sciences and Engineering Research Council of Canada (NSERC) with the award code ALLRP 555053-20.

Conflicts of Interest: The authors declare no conflict of interest.

References

- Ha, Q.P.; Metia, S.; Phung, M.D. Sensing Data Fusion for Enhanced Indoor Air Quality Monitoring. *IEEE Sens. J.* **2020**, *20*, 4430–4441. [CrossRef]
- Jaimini, U.; Banerjee, T.; Romine, W.; Thirunarayan, K.; Sheth, A.; Kalra, M. Investigation of an Indoor Air Quality Sensor for Asthma Management in Children. *IEEE Sens. Lett.* **2017**, *1*, 6000204. [CrossRef]
- World Health Organization (WHO). *Coronavirus Disease (COVID-19) Outbreak: Rights, Roles and Responsibilities of Health Workers, Including Key Considerations for Occupational Safety and Health: Interim Guidance*; WHO: Geneva, Switzerland, 2020.
- World Health Organization. WHO Considers 'Airborne Precautions' for Medical Staff after Study Shows Coronavirus Can Survive in Air. 23 March 2020. Available online: <https://www.cnn.com/2020/03/16/who-considers-airborne-precautions-for-medical-staff-after-study-shows-coronavirus-can-survive-in-air.html> (accessed on 15 February 2020).
- World Health Organization (WHO). *Infection Prevention and Control of Epidemic-and Pandemic-Prone Acute Respiratory Infections in Health Care*; WHO: Geneva, Switzerland, 2014.
- World Health Organization (WHO). Infection Prevention and Control (IPC) for Novel Coronavirus (COVID-19) Course. Available online: <https://openwho.org/courses/COVID-19-IPC-EN> (accessed on 25 December 2020).
- Liu, J.; Liao, X.; Qian, S.; Yuan, J.; Wang, F.; Liu, Y.; Wang, Z.; Wang, F.S.; Liu, L.; Zhang, Z. Community transmission of severe acute respiratory syndrome coronavirus 2, Shenzhen, China, 2020. *Emerg. Infect. Dis.* **2020**, *26*, 132. [CrossRef]
- Chan, J.F.-W.; Yuan, S.; Kok, K.-H.; To, K.K.-W.; Chu, H.; Yang, J.; Xing, F.; Liu, J.; Yip, C.C.-Y.; Poon, R.W.-S.; et al. A familial cluster of pneumonia associated with the 2019 novel coronavirus indicating person-to-person transmission: A study of a family cluster. *Lancet* **2020**, *395*, 514–523. [CrossRef]
- Li, Q.; Guan, X.; Wu, P.; Wang, X.; Zhou, L.; Tong, Y.; Ren, R.; Leung, K.S.; Lau, E.H.; Wong, J.Y.; et al. Early transmission dynamics in Wuhan, China, of novel coronavirus-infected pneumonia. *N. Engl. J. Med.* **2020**, *382*, 1199–1207. [CrossRef]
- Huang, C.; Wang, Y.; Li, X.; Ren, L.; Zhao, J.; Hu, Y.; Zhang, L.; Fan, G.; Xu, J.; Gu, X.; et al. Clinical features of patients infected with 2019 novel coronavirus in Wuhan, China. *Lancet* **2020**, *395*, 497–506. [CrossRef]
- Van Doremalen, N.; Bushmaker, T.; Morris, D.H.; Holbrook, M.G.; Gamble, A.; Williamson, B.N.; Tamin, A.; Harcourt, J.L.; Thornburg, N.J.; Gerber, S.I.; et al. Aerosol and surface stability of SARS-CoV-2 as compared with SARS-CoV-1. *N. Engl. J. Med.* **2020**, *382*, 1564–1567. [CrossRef]
- Morawska, L.; Milton, D.K. It Is Time to Address Airborne Transmission of Coronavirus Disease 2019 (COVID-19). *Clin. Infect. Dis.* **2020**, *71*, 2311–2313. [CrossRef]
- Prather, K.A.; Wang, C.C.; Schooley, R.T. Reducing transmission of SARS-CoV-2. *Science* **2020**, *368*, 1422–1424. [CrossRef]
- Setti, L.; Passarini, F.; De Gennaro, G.; Barbieri, P.; Perrone, M.G.; Borelli, M.; Palmisani, J.; Di Gilio, A.; Piscitelli, P.; Miani, A. Airborne Transmission Route of COVID-19: Why 2 Meters/6 Feet of Inter-Personal Distance Could Not Be Enough. *Int. J. Environ. Res. Public Health* **2020**, *17*, 2932. [CrossRef] [PubMed]
- Liu, Y.; Ning, Z.; Chen, Y.; Guo, M.; Liu, Y.; Gali, N.K.; Sun, L.; Duan, Y.; Cai, J.; Westerdahl, D.; et al. Aerodynamic analysis of SARS-CoV-2 in two Wuhan hospitals. *Nature* **2020**, *582*, 557–560. [CrossRef]
- Asadi, S.; Bouvier, N.; Wexler, A.S.; Ristenpart, W.D. The coronavirus pandemic and aerosols: Does COVID-19 transmit via expiratory particles? *Aerosol Sci. Technol.* **2020**, *54*, 635–638. [CrossRef]
- Megahed, N.A.; Ghoneim, E.M. Indoor Air Quality: Rethinking rules of building design strategies in post-pandemic architecture. *Environ. Res.* **2020**, *193*, 110471. [CrossRef] [PubMed]
- Benamar, B.; Favre, E.; Donnot, A.; Rigo, M. Finite element solution for ionized fields in DC electrostatic precipitator. In Proceedings of the COMSOL Users Conference, Grenoble, France, 23–24 October 2007.
- Shimizu, K.; Kurokawa, Y.; Blajan, M. Basic study of indoor air quality improvement by atmospheric plasma. *IEEE Trans. Ind. Appl.* **2015**, *52*, 1823–1830. [CrossRef]
- Christopherson, D.A.; Yao, W.C.; Lu, M.; Vijayakumar, R.; Sedaghat, A.R. High-Efficiency Particulate Air Filters in the Era of COVID-19: Function and Efficacy. *Otolaryngol. Neck Surg.* **2020**, *163*, 1153–1155. [CrossRef]
- Leder, K.; Newman, D. Respiratory infections during air travel. *Intern. Med. J.* **2005**, *35*, 50–55. [CrossRef] [PubMed]
- Centers for Disease Control and Prevention. SARS-CoV-2 and Potential Airborne Transmission. 2020. Available online: <https://www.cdc.gov/coronavirus/2019-ncov/science/science-briefs/sars-cov-2-transmission.html> (accessed on 1 November 2021).

23. Zhu, S.; Kato, S.; Yang, J.-H. Study on transport characteristics of saliva droplets produced by coughing in a calm indoor environment. *Build. Environ.* **2006**, *41*, 1691–1702. [CrossRef]
24. Liu, L.; Wei, J.; Li, Y.; Ooi, A. Evaporation and dispersion of respiratory droplets from coughing. *Indoor Air* **2017**, *27*, 179–190. [CrossRef]
25. Hinds, W.C. *Aerosol Technology: Properties, Behavior, and Measurement of Airborne Particles*; John Wiley & Sons: Hoboken, NJ, USA, 1999.
26. Zhou, Y.; Ji, S. Experimental and numerical study on the transport of droplet aerosols generated by occupants in a fever clinic. *Build. Environ.* **2021**, *187*, 107402. [CrossRef]
27. Chen, W.; Zhang, N.; Wei, J.; Yen, H.-L.; Li, Y. Short-range airborne route dominates exposure of respiratory infection during close contact. *Build. Environ.* **2020**, *176*, 106859. [CrossRef]
28. Vuorinen, V.; Aarnio, M.; Alava, M.; Alopaeus, V.; Atanasova, N.; Auvinen, M.; Balasubramanian, N.; Bordbar, H.; Erästö, P.; Grande, R.; et al. Modelling aerosol transport and virus exposure with numerical simulations in relation to SARS-CoV-2 transmission by inhalation indoors. *Saf. Sci.* **2020**, *130*, 104866. [CrossRef]
29. Lelieveld, J.; Helleis, F.; Borrmann, S.; Cheng, Y.; Drewnick, F.; Haug, G.; Klimach, T.; Sciare, J.; Su, H.; Pöschl, U. Model Calculations of Aerosol Transmission and Infection Risk of COVID-19 in Indoor Environments. *Int. J. Environ. Res. Public Health* **2020**, *17*, 8114. [CrossRef]
30. Löhner, R.; Antil, H.; Idelsohn, S.; Oñate, E. Detailed simulation of viral propagation in the built environment. *Comput. Mech.* **2020**, *66*, 1093–1107. [CrossRef] [PubMed]
31. Tang, J.W.; Eames, I.; Li, Y.; Taha, Y.A.; Wilson, P.; Bellingan, G.; Ward, K.N.; Breuer, J. Door-opening motion can potentially lead to a transient breakdown in negative-pressure isolation conditions: The importance of vorticity and buoyancy airflows. *J. Hosp. Infect.* **2005**, *61*, 283–286. [CrossRef] [PubMed]
32. Interior Health Authority. IH0200: Airborne Precautions. 2020. Available online: <https://www.interiorhealth.ca/> (accessed on 1 November 2021).
33. United States Environmental Protection Agency. Air Cleaners, HVAC filters, and Coronavirus (COVID-19). 3 April 2019. Available online: <https://www.epa.gov/coronavirus/air-cleaners-hvac-filters-and-coronavirus-covid-19> (accessed on 29 December 2020).
34. Elias, B.; Bar-Yam, Y. Could Air Filtration Reduce COVID-19 Severity and Spread? Available online: <https://necsi.edu/could-air-filtration-reduce-covid19-severity-and-spread> (accessed on 29 December 2020).
35. Zhao, B.; Liu, Y.; Chen, C. Air purifiers: A supplementary measure to remove airborne SARS-CoV-2. *Build. Environ.* **2020**, *177*, 106918. [CrossRef] [PubMed]
36. Chen, L.; Gonze, E.; Ondarts, M.; Outin, J.; Gonthier, Y. Electrostatic precipitator for fine and ultrafine particle removal from indoor air environments. *Sep. Purif. Technol.* **2020**, *247*, 116964. [CrossRef]
37. Feng, Z.; Long, Z.; Yu, T. Filtration characteristics of fibrous filter following an electrostatic precipitator. *J. Electrostat.* **2016**, *83*, 52–62. [CrossRef]
38. Tien, C.Y.; Chen, J.P.; Li, S.; Li, Z.; Zheng, Y.M.; Peng, A.S.; Zhou, F.; Tsai, C.J.; Chen, S.C. Experimental and theoretical analysis of loading characteristics of different electret media with various properties toward the design of ideal depth filtration for nanoparticles and fine particles. *Sep. Purif. Technol.* **2020**, *15*, 116002. [CrossRef]
39. Raynor, P.C.; Chae, S.J. The Long-Term Performance of Electrically Charged Filters in a Ventilation System. *J. Occup. Environ. Hyg.* **2004**, *1*, 463–471. [CrossRef]
40. Podlinski, J.; Niewulsi, A.; Mizeraczyk, J.; Atten, P. ESP performance for various dust densities. *J. Electrostat.* **2008**, *66*, 246–253. [CrossRef]
41. Hackam, R.; Aklyama, H. Air pollution control by electrical discharges. *IEEE Trans. Dielectr. Electr. Insul.* **2000**, *7*, 654–683. [CrossRef]
42. Huang, Y.; Li, S.; Zheng, Q.; Shen, X.; Wang, S.; Han, P.; Liu, Z.; Yan, K. Recent progress of dry electrostatic precipitation for PM_{2.5} emission control from coal-fired boilers. *Int. J. Plasma Environ. Sci. Technol.* **2015**, *9*, 69–85.
43. Popa, G.N.; Abrudean, C.; Deaconu, S.I.; Popa, I.; Vaida, V. A Case Study of ESP Electrical Characteristics from a Thermal Power Station. In Proceedings of the Annual Meeting of the IEEE Industry Applications Society, IAS 2009, Houston, TX, USA, 4–8 October 2009; pp. 1–6.
44. Gao, W.; Wang, Y.; Zhang, H.; Guo, B.; Zheng, C.; Guo, J.; Gao, X.; Yu, A. A Numerical Investigation of the Effect of Dust Layer on Particle Migration in an Electrostatic Precipitator. *Aerosol Air Qual. Res.* **2020**, *20*, 166–179. [CrossRef]
45. Mizuno, A. Electrostatic precipitation. *IEEE Trans. Dielectr. Electr. Insul.* **2000**, *7*, 615–624. [CrossRef]
46. Fujishima, H.; Morita, Y.; Okubo, M.; Yamamoto, T. Numerical simulation of three-dimensional electrohydrodynamics of spiked-electrode electrostatic precipitators. *IEEE Trans. Dielectr. Electr. Insul.* **2006**, *13*, 160–167. [CrossRef]
47. Jaworek, A.K.; Czech, T. Modern electrostatic devices and methods for exhaust gas cleaning: A brief review. *J. Electrostat.* **2007**, *65*, 133–155. [CrossRef]
48. Chang, J.S. Next generation integrated electrostatic gas cleaning systems. *J. Electrostat.* **2003**, *57*, 273–291. [CrossRef]
49. Parker, K.R. *Applied Electrostatic Precipitators*; Chapman and Hall: London, UK, 1997; pp. 192–229.
50. Kuffel, J.; Kuffel, E. *High Voltage Engineering: Fundamentals*; Elsevier: Oxford, UK, 2000; pp. 129–171.
51. Robinson, M. Electrostatic precipitation. In *Air Pollution Control*; Strauss, W., Ed.; Wiley-Interscience: New York, NY, USA, 1971.
52. White, K.J. *Industrial Electrostatic Precipitation*; Addison-Wesley: Reading, MA, USA, 1963.

53. Rose, H.E.; Wood, A.J. *An Introduction to Electrostatic Precipitators*, 2nd ed.; Constable: London, UK, 1966.
54. Oglesby, S.; Nichols, G.B. *Electrostatic Precipitation*; Marcel Dekker: New York, NY, USA, 1978.
55. White, H.J. Electrostatic precipitation of fly ash. *J. Air Pollut. Con. Assoc.* **1977**, *27*, 15–22. [[CrossRef](#)]
56. Grass, N.; Hartmann, W.; Klöckner, M. Application of Different Types of High-Voltage Supplies on Industrial Electrostatic Precipitators. *IEEE Trans. Ind. Appl.* **2004**, *40*, 1513–1520. [[CrossRef](#)]
57. Jędrusik, M.; Gajewski, J.B.; Świerczok, A.J. Effect of the particle diameter and corona electrode geometry on the particle migration velocity in electrostatic precipitators. *J. Electrostat.* **2001**, *51–52*, 245–251. [[CrossRef](#)]
58. Dumitran, L.; Blejan, O.; Notingher, P.; Samuila, A.; Dascalescu, L. Particle Charging in Combined Corona-Electrostatic Fields. *IEEE Trans. Ind. Appl.* **2008**, *44*, 1385–1390. [[CrossRef](#)]
59. Popa, G.N.; Diniş, C.M.; Deaconu, S.I. Numerical Modelling in Plate-Type Electrostatic Precipitator Supplied with Pulse Energization. In Proceedings of the 2011—14th European Conference on Power Electronics and Applications, EPE 2011, Birmingham, UK, 30 August–1 September 2011; pp. 1–8.
60. Popa, G.N.; Diniş, C.M.; Deaconu, S.I.; Popa, A. Numerical Modeling of Electric Parameters from Industrial Plate-Type Electrostatic Precipitator. In Proceedings of the 2011 IEEE International Conference on Industrial Technology ICIT 2011 IEEE, Auburn, AL, USA, 14–16 March 2011; pp. 21–26.
61. Lobry, J. A New Numerical Scheme for the Simulation of Corona Fields. *IEEE Trans. Magn.* **2014**, *50*, 541–544. [[CrossRef](#)]
62. Butler, A.J.; Cendes, Z.J.; Hoburg, J.F. Interfacing the finite-element method with the method of characteristics in self-consistent electrostatic field models. *IEEE Trans. Ind. Appl.* **1989**, *25*, 533–538. [[CrossRef](#)]
63. Riediker, M.; Tsai, D.-H. Estimation of Viral Aerosol Emissions from Simulated Individuals with Asymptomatic to Moderate Coronavirus Disease 2019. *JAMA Netw. Open* **2020**, *3*, e2013807. [[CrossRef](#)]
64. Asadi, S.; Wexler, A.S.; Cappa, C.; Barreda, S.; Bouvier, N.M.; Ristenpart, W.D. Effect of voicing and articulation manner on aerosol particle emission during human speech. *PLoS ONE* **2020**, *15*, e0227699. [[CrossRef](#)]
65. Nicas, M.; Nazaroff, W.; Hubbard, A. Toward Understanding the Risk of Secondary Airborne Infection: Emission of Respirable Pathogens. *J. Occup. Environ. Hyg.* **2005**, *2*, 143–154. [[CrossRef](#)]
66. Wells, W.F. *Airborne Contagion and Air Hygiene: An Ecological Study of Droplet Infections*; Harvard University Press: Cambridge, MA, USA, 1955.
67. Mittal, R.; Ni, R.; Seo, J.-H. The flow physics of COVID-19. *J. Fluid Mech.* **2020**, *894*, F2. [[CrossRef](#)]
68. Atkinson, J.; Chartier, Y.; Pessoa-Silva, C.L.; Jensen, P.; Li, Y.; Seto, W.-H. *Natural Ventilation for Infection Control in Health-Care Settings*; World Health Organization: Geneva, Switzerland, 2009.
69. Dhand, R.; Li, J. Coughs and Sneezes: Their Role in Transmission of Respiratory Viral Infections, Including SARS-CoV-2. *Am. J. Respir. Crit. Care Med.* **2020**, *202*, 651–659. [[CrossRef](#)]
70. Dolata, M.; Michalski, J. Non-linear effects in spherical particle motion in oscillatory flowing gas. *Pol. J. Chem.* **1999**, *73*, 347–357.
71. Clift, R.; Grace, J.R.; Weber, M.E. *Bubbles, Drops, and Particles*; Dover: Mineola, NY, USA, 2005.
72. Xie, X.; Li, Y.; Chwang, A.T.Y.; Ho, P.L.; Seto, W.H. How far droplets can move in indoor environments—Revisiting the Wells evaporation—falling curve. *Indoor Air* **2007**, *17*, 211–225. [[CrossRef](#)]
73. Wells, W.F. On air-borne infection: Study II: Droplets and droplet nuclei. *Am. J. Hyg.* **1934**, *20*, 611–618.
74. Ai, Z.T.; Melikov, A.K. Airborne spread of expiratory droplet nuclei between the occupants of indoor environments: A review. *Indoor Air* **2018**, *28*, 500–524. [[CrossRef](#)]
75. Bahl, P.; Doolan, C.; DE Silva, C.; Chughtai, A.A.; Bourouiba, L.; MacIntyre, C.R. Airborne or Droplet Precautions for Health Workers Treating Coronavirus Disease 2019? *J. Infect. Dis.* **2020**, jiaa189. Available online: <https://academic.oup.com/jid/advance-article/doi/10.1093/infdis/jiaa189/5820886> (accessed on 1 November 2021). [[CrossRef](#)]
76. Blocken, B.; van Druenen, T.; Ricci, A.; Kang, L.; van Hooff, T.; Qin, P.; Xia, L.; Ruiz, C.A.; Arts, J.; Diepens, J.; et al. Ventilation and air cleaning to limit aerosol particle concentrations in a gym during the COVID-19 pandemic. *Build. Environ.* **2021**, *193*, 107659. [[CrossRef](#)]
77. Zhu, Z.; Momeu, C.; Zakhartsev, M.; Schwaneberg, U. Making glucose oxidase fit for biofuel cell applications by directed protein evolution. *Biosens. Bioelectron.* **2006**, *21*, 2046–2051. [[CrossRef](#)]
78. Morawska, L.; Johnson, G.; Ristovski, Z.; Hargreaves, M.; Mengersen, K.; Corbett, S.; Chao, Y.H.C.; Li, Y.; Katoshevski, D. Size distribution and sites of origin of droplets expelled from the human respiratory tract during expiratory activities. *J. Aerosol Sci.* **2009**, *40*, 256–269. [[CrossRef](#)]
79. Redrow, J.; Ma, L.; Celik, I.; Posada, J.; Feng, Z.-G. Modeling the evaporation and dispersion of airborne sputum droplets expelled from a human cough. *Build. Environ.* **2011**, *46*, 2042–2051. [[CrossRef](#)]
80. Vejerano, E.P.; Marr, L.C. Physico-chemical characteristics of evaporating respiratory fluid droplets. *J. R. Soc. Interface* **2018**, *15*, 20170939. [[CrossRef](#)]
81. Schade, W.; Reimer, V.; Seipenbusch, M.; Willer, U. Experimental Investigation of Aerosol and CO₂ Dispersion for Evaluation of COVID-19 Infection Risk in a Concert Hall. *Int. J. Environ. Res. Public Health* **2021**, *18*, 3037. [[CrossRef](#)] [[PubMed](#)]
82. Centers for Disease Control and Prevention. Transmission-Based Precautions. CDC. Available online: <https://www.cdc.gov/infectioncontrol/basics/transmission-based-precautions.html> (accessed on 1 November 2021).
83. Dbouk, T.; Drikakis, D. On respiratory droplets and face masks. *Phys. Fluids* **2020**, *32*, 063303. [[CrossRef](#)]

84. Chen, C.; Ji, W.; Zhao, B. Size-dependent efficiencies of ultrafine particle removal of various filter media. *Build. Environ.* **2019**, *160*, 106171. [[CrossRef](#)]
85. Kallio, G.A.; Stock, D.E. Computation of electrical conditions inside wire-duct electrostatic precipitators using a combined finite-element, finite-difference technique. *J. Appl. Phys.* **1986**, *59*, 1799–1806. [[CrossRef](#)]
86. Farnoosh, N. Three-Dimensional Modeling of Electrostatic Precipitator Using Hybrid Finite Element-Flux Corrected Transport Technique. Ph.D. Thesis, The University of Western Ontario, London, ON, Canada, 2011.
87. Peek, E. *Determination Phenomena in High Voltage*; McGraw-Hill: New York, NY, USA, 1929; pp. 52–80.
88. Beroual, A.; Fofana, I. *Discharge in Long Air Gap—Modeling and Applications*; IOP Publishing: Bristol, UK, 2016; Available online: <http://iopscience.iop.org/book/978-0-7503-1236-3> (accessed on 1 November 2021).
89. Shah, K.P. Construction, Working, Operation and Maintenance of Electrostatic Precipitators (ESPs). 2017. Available online: <https://practicalmaintenance.net/wp-content/uploads/Construction-Working-Operation-and-Maintenance-of-Electrostatic-Precipitators-ESPs.pdf> (accessed on 1 November 2021).
90. Chu, P.K.; Lu, X. *Low Temperature Plasma Technology: Methods and Applications*; CRC Press: Boca Raton, FL, USA, 2013.
91. Huang, S.-H.; Chen, C.-C. Ultrafine Aerosol Penetration through Electrostatic Precipitators. *Environ. Sci. Technol.* **2002**, *36*, 4625–4632. [[CrossRef](#)]
92. Podlinski, J.; Kocik, M.; Barbucha, R.; Niewulis, A.; Mizeraczyk, J.; Mizuno, A. 3D PIV measurements of the EHD flow patterns in a narrow electrostatic precipitator with wire-plate or wire-flocking electrodes. *Czechoslov. J. Phys.* **2006**, *56*, B1009–B1016. [[CrossRef](#)]
93. Oglesby, S., Jr.; Nichols, G.B. Electrostatic precipitation. *Air Pollut.* **2014**, *24*, 189–256.
94. Arrondel, V.; Bacchiega, G.; Hamilil, M. The electrostatic precipitator external parameters at the heart of dust collection efficiency performance: Coal characteristics, combustion quality and SCR chemical process. In Proceedings of the 12th International Conference on Electrostatic Precipitation, Nuremberg, Germany, 12–13 May 2011; pp. 25–32.
95. Lee, Y.; Sung, J.H.; Han, B.; Kim, Y.J.; Kim, H.J. Particle removal performance of a two stage electrostatic precipitator with carbon based nonmetallic collection plates for oil mist. In Proceedings of the 2020 IEEE Industry Applications Society Annual Meeting, Detroit, MI, USA, 11–15 October 2020; pp. 1–7.
96. Kim, Y.J.; Han, B.; Woo, C.G.; Kim, H.J. Performance of ultrafine particle collection of a two-stage ESP using a novel mixing type carbon brush charger and parallel collection plates. *IEEE Trans. Ind. Appl.* **2016**, *53*, 466–473. [[CrossRef](#)]
97. Yoo, K.H.; Lee, J.S.; Oh, M.D. Charging and collection of submicron particles in two-stage parallel-plate electrostatic precipitators. *Aerosol Sci. Technol.* **1997**, *27*, 308–323. [[CrossRef](#)]
98. Kim, H.J.; Kim, M.; Han, B.; Woo, C.G.; Zouaghi, A.; Zouzou, N.; Kim, Y.J. Fine particle removal by a two-stage electrostatic precipitator with multiple ion-injection-type prechargers. *J. Aerosol Sci.* **2019**, *130*, 61–75. [[CrossRef](#)]
99. Kim, Y.-J.; Han, B.; Woo, C.G.; Kim, H.-J. Ultrafine Particle Collection Performance of a Two-Stage ESP With a Novel Mixing-Type Charging Stage Using Different Geometries and Electrical Conditions. *IEEE Trans. Ind. Appl.* **2017**, *53*, 5859–5866. [[CrossRef](#)]
100. Jaworek, A.; Sobczyk, A.T.; Marchewicz, A.; Krupa, A.; Czech, T.; Charchalis, A. Two-stage vs. two-field electrostatic precipitator. *J. Electrostat.* **2017**, *90*, 106–112. [[CrossRef](#)]
101. Ji, J.-H.; Hwang, J.; Bae, G.-N.; Kim, Y.-G. Particle charging and agglomeration in DC and AC electric fields. *J. Electrostat.* **2004**, *61*, 57–68. [[CrossRef](#)]
102. Chen, H.; Luo, Z.; Jiang, J.; Zhou, D.; Lu, M.; Fang, M.; Cen, K. Effects of simultaneous acoustic and electric fields on removal of fine particles emitted from coal combustion. *Powder Technol.* **2015**, *281*, 12–19. [[CrossRef](#)]
103. Chang, Q.; Zheng, C.; Yang, Z.; Fang, M.; Gao, X.; Luo, Z.; Cen, K. Electric agglomeration modes of coal-fired fly-ash particles with water droplet humidification. *Fuel* **2017**, *200*, 134–145. [[CrossRef](#)]
104. Wang, X.; Chang, J.; Xu, C.; Zhang, J.; Wang, P.; Ma, C. Collection and charging characteristics of particles in an electrostatic precipitator with a wet membrane collecting electrode. *J. Electrostat.* **2016**, *83*, 28–34. [[CrossRef](#)]
105. Rubinetti, D.; Weiss, D.; Egli, W. Corona Discharge—A Fully Coupled Numerical Approach Verified and Validated. *Int. J. Multiphysics* **2017**, *11*, 375–386.
106. Haque, S.M.; Rasul, M.G.; Khan, M.M.K.; Deev, A.V.; Subaschandar, N. A numerical model of an electrostatic precipitator. In Proceedings of the 16th Australasian Fluid Mechanics Conference, Gold Coast, Australia, 2–7 December 2007.
107. Choi, B.; Fletcher, C. Turbulent particle dispersion in an electrostatic precipitator. *Appl. Math. Model.* **1998**, *22*, 1009–1021. [[CrossRef](#)]
108. Lieberman, M.A.; Lichtenberg, A.J. *Principles of Plasma Discharges and Materials Processing*; Wiley: Hoboken, NJ, USA, 2005.
109. Munson, B.; Young, D.F.; Okiishi, T.H. *Fundamentals of Fluids Mechanics*, 4th ed.; John Wiley & Sons: New York, NY, USA, 2002; p. 833.